

## Hierarchical Self-Supported TiO<sub>2</sub>/NC-MoS<sub>2</sub> Composite as a Stable Anode for Enhanced Lithium-Ion Batteries

Peng Sun<sup>1</sup>, Haigang Liu<sup>1</sup>, Xiankun Ma<sup>1</sup>, Jiahua Zhao<sup>1</sup>, Junlin Qiu<sup>1</sup>, Yongfei Wang<sup>1,2,\*</sup>, Zhiqiang Zhang<sup>1,\*</sup>

<sup>1</sup> School of Chemical Engineering, University of Science and Technology Liaoning, 185#, Qianshan Zhong Road, Anshan 114044, PR China

<sup>2</sup> School of Materials and Metallurgy, University of Science and Technology Liaoning, 185#, Qianshan Zhong Road, Anshan 114044, PR China

\*E-mail: [wyf8307@ustl.edu.cn](mailto:wyf8307@ustl.edu.cn), [zzq@ustl.edu.cn](mailto:zzq@ustl.edu.cn)

Received: 26 April 2020 / Accepted: 29 May 2020 / Published: 10 July 2020

---

Ultrafine MoS<sub>2</sub> nanosheets are embedded with nitrogen-doped carbon-coated TiO<sub>2</sub> nanofibers (TiO<sub>2</sub>/NC-MoS<sub>2</sub>) via a facile hydrothermal reaction and annealing treatment. Applied in the anode of a lithium-ion battery, the as-prepared TiO<sub>2</sub>/NC-MoS<sub>2</sub> hybrid delivers a good cycling performance of 629.9 mA h g<sup>-1</sup> at 0.1 A g<sup>-1</sup> after 200 cycles and a rate capability of 471.2 mA h g<sup>-1</sup> at 1 A g<sup>-1</sup> over 1000 cycles. The superior electrochemical performance results from both the unique hierarchical morphology and the synergic effects among various interfaces and components. Nitrogen doping in carbon materials can facilitate the transfer of Li ions and TiO<sub>2</sub> nanofibers to prevent the aggregation of MoS<sub>2</sub> nanosheets. The MoS<sub>2</sub> nanosheets provide more active sites for electrochemical reactions. This work demonstrates that the obtained composite holds great potential for high-performance energy storage applications.

---

**Keywords:** MoS<sub>2</sub>, hydrothermal, electrochemical, anode

### 1. INTRODUCTION

Lithium-ion batteries (LIBs) have been intensively studied and applied in electric products due to their low cost and lack of pollution. [1-3] Graphite is a typical anode material; however, its low capacity cannot meet the future demand for large-scale applications in batteries. To date, many studies have investigated developing substitutes with increased energy density and safety.[4-6] Transition-metal oxides and sulfides have attracted great interest in terms of achieving improved anodes.[7,8] As a typical 2D metal sulfide, molybdenum disulfide (MoS<sub>2</sub>), which has a layered structure with layer spacings of 0.62 nm, is good for Li<sup>+</sup> embedding; thus, it is a good anode material for LIBs.[9,10] One challenge is that the strength of MoS<sub>2</sub> nanosheets is too low to endure the great stress variation accompanying the

discharge and charge process, which results in severe restacking and structural pulverization, with fast capacity fading. [11, 12]

Interconversion-type  $\text{TiO}_2$  has been proposed as an excellent material owing to its long cycle life, nontoxicity and low cost. Moreover, there is very little volume expansion (<4%) during the Li insertion/extraction process. However, the low lithium-ion diffusivity and electronic conductivity restrict the applications of such a material. [13,14]  $\text{TiO}_2$  has been generally applied as a composite substrate, and the strength of  $\text{MoS}_2$ -based electrode materials may be improved by the integration of  $\text{TiO}_2$ . [15-17] Several  $\text{MoS}_2/\text{TiO}_2$  composites have been reported very recently. One example involved filling ultrathin  $\text{MoS}_2$  nanosheets into the nanoscale voids of  $\text{TiO}_2$  microspheres, which were then encased with graphene.[18]  $\text{TiO}_2/\text{MoS}_2$  nanofibers were synthesized through  $\text{MoS}_2$  nanoparticles wrapped in a  $\text{TiO}_2$  nanofibrous backbone via a facile method.[19] The preparation of core-shell  $\text{TiO}_2@\text{MoS}_2$  was reported by using thin titania nanosheets coated with  $\text{MoS}_2$  shells.[20] Fish-scale-like  $\text{MoS}_2$  could be decorated in the interspace of flower-like  $\text{TiO}_2/\text{C}$  microspheres.[21] While the Li storage has been enhanced in these examples, these nanohybrid anodes are still subject to the inferior intrinsic conductivity of  $\text{TiO}_2$  and  $\text{MoS}_2$ . Recently, some researchers have discovered the benefits of N-doping in carbon materials, specifically in electrode materials.[22-24] Doping with nitrogen can improve the electronic properties by providing more active sites and ion diffusion pathways.[25,26] Polydopamine (PDA) is a catecholamine polymer derived from the oxidation polymerization of dopamine.[27] Carbonized PDA with a high nitrogen content can release volumetric strains and display high electrical conductivity.[28-29]  $\text{MoS}_2@\text{TiO}_2$  nanofiber hybrid nanostructures have been prepared with a template-assisted hydrothermal approach, and they present good electrochemical performance.[30] However, the complicated synthesis procedure requires removal of the template by methods such as calcination at high temperature or etching in harsh solutions, thus restricting the following applications.

Based on the above considerations, a rational structure of  $\text{MoS}_2/\text{TiO}_2$  nanomaterials still needs to be designed, which would enable many advantages in one hybrid material. Herein, we report the preparation of a  $\text{MoS}_2$  hybrid with N-doped carbon-coated  $\text{TiO}_2$  ( $\text{TiO}_2/\text{NC}-\text{MoS}_2$ ) via a simple and economical PDA-assisted carbonization and hydrothermal process. Benefiting from the merits of 1D  $\text{TiO}_2$  nanofibers and 2D  $\text{MoS}_2$  nanosheets, the hybrids can integrate the high capacity of  $\text{MoS}_2$  and superior cycling stability of  $\text{TiO}_2$ . In addition, PDA can provide carbon and nitrogen sources, and the introduction of PDA can improve the rate capacity by increasing the conductivity. Thus, the prepared  $\text{TiO}_2/\text{NC}-\text{MoS}_2$  anodes exhibit excellent cycling performance and outstanding high-rate capability. The  $\text{TiO}_2/\text{NC}-\text{MoS}_2$  composite delivers a high discharge capacity of  $649.4 \text{ mA h g}^{-1}$  at  $0.1 \text{ A g}^{-1}$  and exhibits outstanding cycling stability, with a capacity retention of 97% after 200 cycles.

## 2. EXPERIMENTAL

### 2.1 Synthesis of $\text{TiO}_2/\text{NC}-\text{MoS}_2$ , $\text{TiO}_2/\text{NC}$ and $\text{MoS}_2$

$\text{TiO}_2$  nanofibers were prepared as previously described.[31]  $\text{TiO}_2$  (130 mg) was added to Tris-HCl (200 mL), and then, dopamine (30 mg) was added to the solution. The mixture was stirred for 3 h.

Afterwards, the product was rinsed with ethanol and deionized water and then dried at 60°C for 12 h. TiO<sub>2</sub>/PDA was carbonized at 300°C for 3 h under an Ar atmosphere at a heating rate of 3°C min<sup>-1</sup>. The product TiO<sub>2</sub>/NC was obtained.

TiO<sub>2</sub>/NC-MoS<sub>2</sub> was obtained by a hydrothermal method. TiO<sub>2</sub>/NC was added to a glucose solution (0.1 M, 40 mL). Then, NaMoO<sub>4</sub>·2H<sub>2</sub>O (80 mg) and thiourea (160 mg) were added and stirred for 0.5 h. Next, the hydrothermal reaction was performed at 180°C for 12 h. The sample was rinsed with a large amount of deionized water and dried. The product was heated at 700°C at 5°C min<sup>-1</sup> in a N<sub>2</sub> atmosphere for 1 h. Black powder was obtained. Pristine MoS<sub>2</sub> and TiO<sub>2</sub>/NC were synthesized using a similar procedure.

## 2.2 Characterization

The products were characterized by X-ray diffraction (XRD, X'Pert PRO, PANalytical B.V., Cu K $\alpha$  radiation,  $\lambda=1.5418$  Å), transmission electron microscopy (TEM, JEM-2010F, JEOL, Japan), Raman spectroscopy (Jobin Yvon LabRam HR800, excitation wavelength 532 nm), X-ray photoelectron spectroscopy (XPS, Newcastle, U.K.), scanning electron microscopy (SEM, Carl Zeiss AG, Germany), and nitrogen adsorption-desorption isotherms (Quantachrome, USA).

## 2.3 Electrochemical performance

The electrochemical performance was assessed with a 2032-type half coin cell. The products were mixed with carbon black and polyvinylidene fluoride (PVDF) (mass ratio= 80:10:10) in N-methylpyrrolidone and then cured on copper foil. The electrolyte was mixed ethylene carbonate (EC) and diethyl carbonate (DEC) containing 1 M LiPF<sub>6</sub>. Cyclic voltammetry (CV) was performed from 0.01–3.0 V on a Vertex.C DC electrochemical workstation (Metrohm, Netherlands). Electrochemical impedance spectroscopy (EIS) was also performed (100 kHz~0.01 Hz). The galvanostatic charge-discharge test was conducted under the following conditions: scan rate of 0.2 mv s<sup>-1</sup> and voltage range of 0.01–3.0 V at 25°C (LAND-CT2001A battery-testing instrument).

## 3. RESULTS AND DISCUSSION

The synthetic route of the TiO<sub>2</sub>/NC-MoS<sub>2</sub> nanocomposite is shown in Fig. 1. First, TiO<sub>2</sub>/NC was synthesized by PDA coating, followed by calcination in an Ar atmosphere. Then, the MoS<sub>2</sub> nanosheets grew on the surface of TiO<sub>2</sub>/NC nanowires with the assistance of glucose through the hydrothermal reaction. The hydrothermal sample was treated at 700°C under a N<sub>2</sub> atmosphere to obtain the annealed TiO<sub>2</sub>/NC-MoS<sub>2</sub> hybrid.

The crystallographic properties of TiO<sub>2</sub>/NC-MoS<sub>2</sub> and TiO<sub>2</sub>/NC were analyzed based on the XRD patterns (Fig. 2a). The diffraction pattern revealed that anatase TiO<sub>2</sub> (JPCDS: No. 21-1272), TiO<sub>2</sub>-B (JPCDS: No. 46-1238), and hexagonal MoS<sub>2</sub> phase (JCPDS: No. 37-1492) were obtained. [32,33] The (002), (100), and (110) peaks of hexagonal MoS<sub>2</sub> appeared after the hydrothermal and carbonization

processes, indicating the successful coexistence of MoS<sub>2</sub> and TiO<sub>2</sub>. [34] Notably, the (002) diffraction peak at 14° corresponding to the c plane of MoS<sub>2</sub> was absent. This result indicated that the MoS<sub>2</sub> nanosheets along the TiO<sub>2</sub> nanofibers were not in a stacked arrangement, and they contained few-layered MoS<sub>2</sub> nanosheets. [35] The obvious peaks at 2θ values of 25.3, 37.8 and 53.9° were assigned to the (101), (004) and (105) planes of the anatase TiO<sub>2</sub> phase, respectively, becoming sharper and more intense than those for TiO<sub>2</sub>/NC, which indicated that the crystallinity of the sample was slightly improved after annealing.

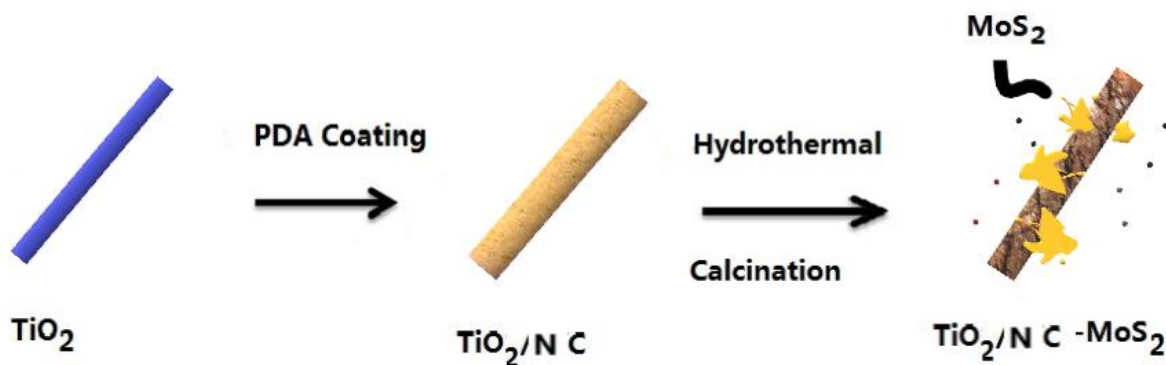


Figure 1. The synthetic route of TiO<sub>2</sub>/NC-MoS<sub>2</sub>

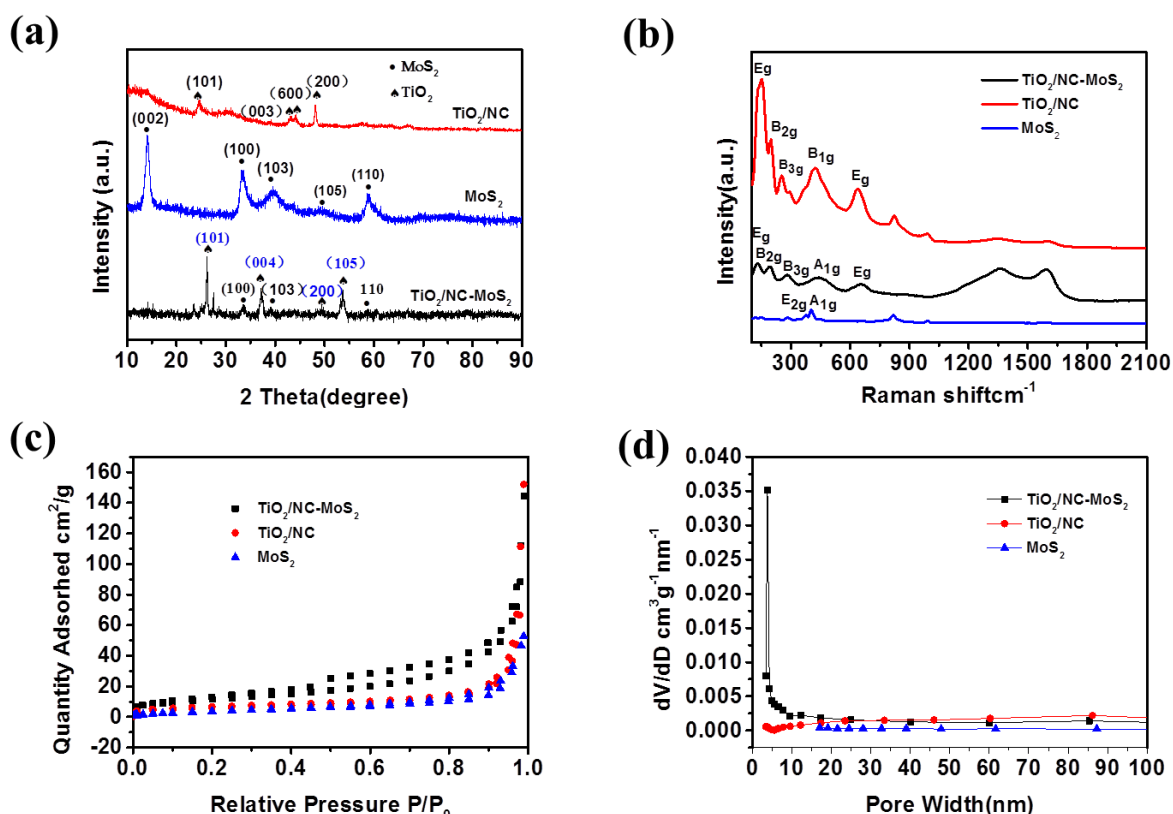
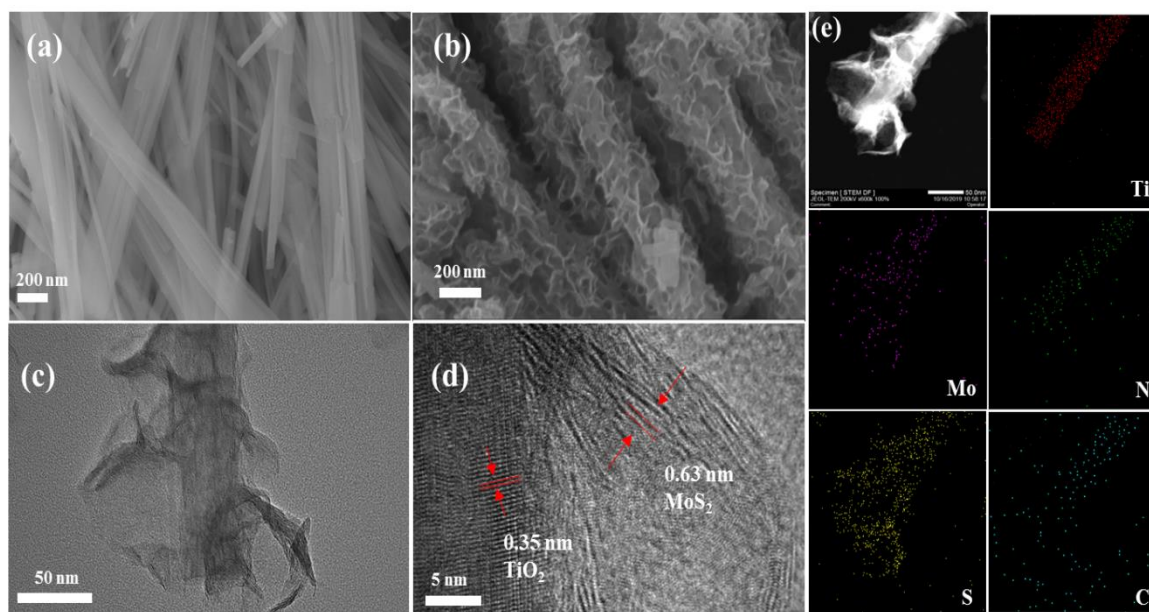


Figure 2. (a) XRD patterns, (b) Raman spectra, (c) N<sub>2</sub> adsorption/desorption isotherms, and (d) pore size distributions of the TiO<sub>2</sub>@NC-MoS<sub>2</sub> hybrids, TiO<sub>2</sub>@NC and MoS<sub>2</sub>.

The Raman spectrum is depicted in Fig. 2b. Four peaks at 151, 198, 254 and 643  $\text{cm}^{-1}$  are assigned to the  $E_g$ ,  $B_{2g}$ ,  $B_{3g}$  and  $E_g$  bands of  $\text{TiO}_2$ , respectively.[31,36] In addition, the peak at 420  $\text{cm}^{-1}$  was due to the  $A_{1g}$  mode of  $\text{MoS}_2$ , suggesting that  $\text{MoS}_2$  was successfully embedded in the  $\text{TiO}_2/\text{NC}$  nanofiber. Moreover, a blueshift of the  $E_{2g}$  mode of  $\text{MoS}_2$  was observed for the composite, which was probably owing to the surface strain induced by the  $\text{MoS}_2$  decorated on the surface of the  $\text{TiO}_2/\text{NC}$  nanofiber. [37,38] Two peaks at 1358  $\text{cm}^{-1}$  and 1593  $\text{cm}^{-1}$ , which were attributed to the D band and G band, respectively, demonstrated the existence of carbon.[38] The intensity ratio  $I_D/I_G$  was calculated to be 1.27, indicating a low graphitic degree. [40]

The  $\text{N}_2$  adsorption-desorption results showed the BET-based surface area (Fig 2. 3c), which was 21.6  $\text{m}^2 \cdot \text{g}^{-1}$  and 14.1  $\text{m}^2 \cdot \text{g}^{-1}$  for  $\text{TiO}_2/\text{NC}$  and  $\text{MoS}_2$ , respectively, and 41.7  $\text{m}^2 \cdot \text{g}^{-1}$  for the  $\text{TiO}_2/\text{NC}-\text{MoS}_2$  hybrid. The  $\text{TiO}_2$  nanofibers suppressed the stacking of  $\text{MoS}_2$ , and the surface area of the hybrid was further enlarged by the regular growth of  $\text{MoS}_2$  nanosheets. The BJH plots showed that the  $\text{TiO}_2/\text{NC}-\text{MoS}_2$  hybrid is in the mesoporous range, with a sharp peak at 3.5 nm.



**Figure 3.** SEM images of (a)  $\text{TiO}_2$  nanofibers, (b)  $\text{TiO}_2/\text{NC}-\text{MoS}_2$  hybrids, (c) high-magnification TEM images, (d) HRTEM images, and (e) TEM-EDS mapping of the as-synthesized  $\text{TiO}_2/\text{NC}-\text{MoS}_2$  hybrids.

The morphology of the prepared samples is presented in Fig. 3a. The diameter of the  $\text{TiO}_2$  nanotubes was approximately 200 nm, presenting a smooth surface. As shown in Fig. 3b, a layer of  $\text{MoS}_2$  nanosheets is uniformly coated on the  $\text{TiO}_2$  nanotubes after the solvothermal and carbonization processes. Fig. 2c clearly shows the hierarchical structure of the  $\text{TiO}_2/\text{NC}-\text{MoS}_2$  composite surface. From the HRTEM image in Fig. 3d, the (002) planes of  $\text{MoS}_2$  and (101) planes of anatase  $\text{TiO}_2$  can be observed, indicating a well-defined structure and heterojunction. Molybdenum, titanium, oxygen and

sulfur can be found in the elemental mappings, proving that TiO<sub>2</sub>/NC-MoS<sub>2</sub> composites were obtained (Fig. 3e). [41]

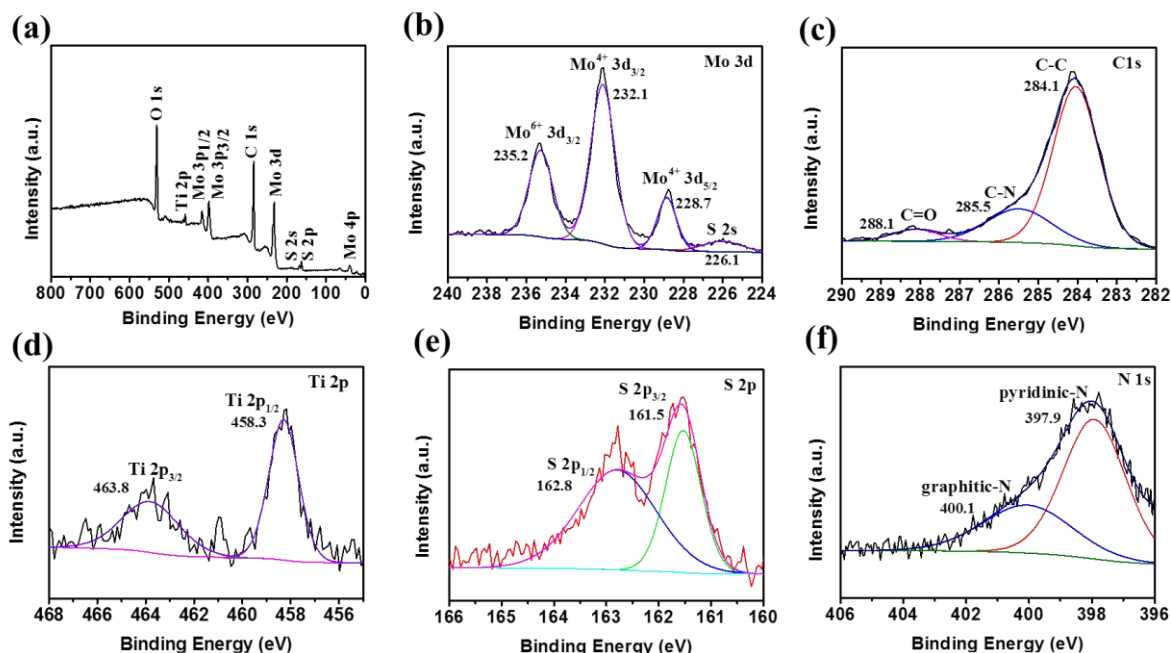


**Figure 4.** XPS spectra of TiO<sub>2</sub>/NC-MoS<sub>2</sub>: (a) survey scan, (b) Mo 3d, (c) C 1s, (d) Ti 2p, (e) S 2p and (f) N 1s

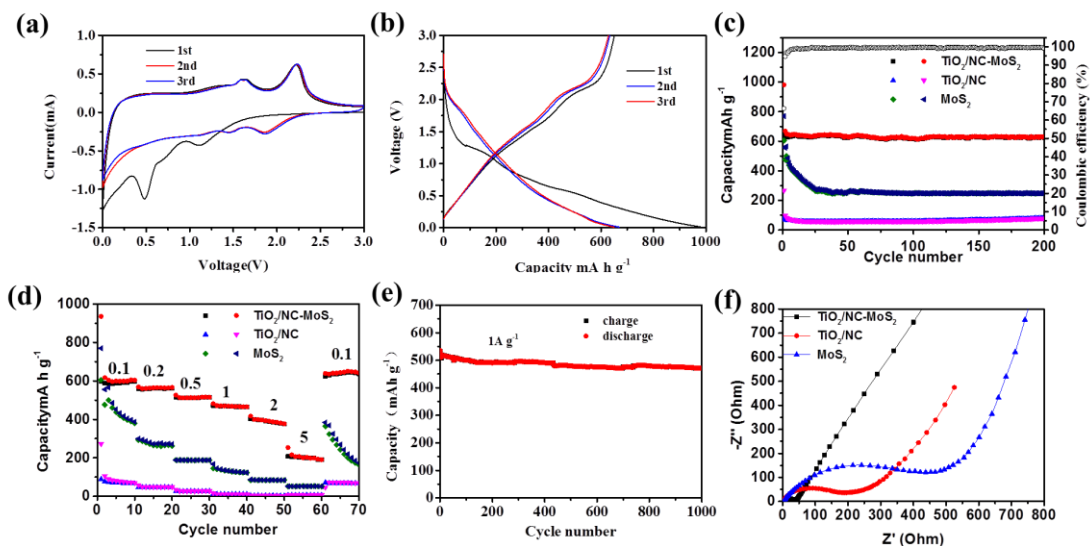


**Figure 5.** Electrochemical tests: a) CV curves at 0.01-3 mVs<sup>-1</sup> with a scan rate of 0.2 mV s<sup>-1</sup>. b) Galvanostatic charge-discharge profiles from the 1<sup>st</sup> to 3<sup>rd</sup> cycle at current densities of 0.1 A g<sup>-1</sup>. c) Cycling performance. d) Rate capability. e) Long cycling performance (1 A g<sup>-1</sup>) of the TiO<sub>2</sub>/NC-MoS<sub>2</sub> composite electrode. f) Nyquist plots of the TiO<sub>2</sub>/NC-MoS<sub>2</sub> hybrids, TiO<sub>2</sub>/NC and MoS<sub>2</sub>.

To analyze the chemical components of the TiO<sub>2</sub>/NC-MoS<sub>2</sub> hybrid, XPS was performed (Fig. 4). There were characteristic peaks of Mo, Ti, C, S, O and N. In the high-resolution Mo 3d spectra, the peaks at 232.1 and 228.7 eV corresponded to Mo 3d<sub>3/2</sub> and Mo 3d<sub>5/2</sub>, respectively. The peak at 235.2 eV resulted from the oxidation of molybdenum.[42] In the high-resolution C 1s spectrum (Fig. 4c), there was an obvious peak of graphitic C at 284.1 eV. The peaks at 285.5 and 288.1 eV corresponded to C–N and C=O bonds, respectively. The peaks of the Ti 2p spectrum included Ti 2p<sub>1/2</sub> at 458.3 eV and Ti 2p<sub>3/2</sub> at 463.8 eV (Fig. 4d), which correspond to the classic values for TiO<sub>2</sub>. [43] For S 2p, the S<sup>2-</sup> 2p<sub>3/2</sub> and S<sup>2-</sup> 2p<sub>1/2</sub> of the TiO<sub>2</sub>/NC/MoS<sub>2</sub> composites were at 161.5 and 162.8 eV, respectively, which is consistent with a previous report.[44] For the N 1s spectrum, there were two nitrogen species: pyridinic-N at 397.9 eV and graphitic-N at 400.1 eV (Fig. 4f), and the introduction of nitrogen-doped carbon was good for ion and electron transport.[45]

The CV behavior of the TiO<sub>2</sub>/NC-MoS<sub>2</sub> composite is in good agreement with the behavior of other previously reported TiO<sub>2</sub>/MoS<sub>2</sub> materials.[46] In the primary discharge process of the TiO<sub>2</sub>/NC-MoS<sub>2</sub>-based electrode material, the reduction peaks at 0.71 V indicate that Li<sup>+</sup> was inserted into the MoS<sub>2</sub> layers to form Li<sub>x</sub>MoS<sub>2</sub> based on the following process:[47] MoS<sub>2</sub>+xLi<sup>+</sup>+x e<sup>-</sup>→Li<sub>x</sub>MoS<sub>2</sub>. The peak at 0.48 V corresponds to further conversion of Li<sub>x</sub>MoS<sub>2</sub> into Mo and Li<sub>2</sub>S:[48] Li<sub>x</sub>MoS<sub>2</sub>+(4-x)Li<sup>+</sup>+(4-x)e<sup>-</sup>→Mo+2Li<sub>2</sub>S. In addition, in the CV curves, the two reduction peaks disappeared after the first discharge, indicating that the conversion of MoS<sub>2</sub> to Li<sub>2</sub>S and Mo was irreversible. The peak at 1.12 V is attributed to Li<sup>+</sup> embedded in TiO<sub>2</sub>, which causes TiO<sub>2</sub> to convert to Li<sub>x</sub>TiO<sub>2</sub> via the following reaction:[49,50] TiO<sub>2</sub>+xLi<sup>+</sup>+x e<sup>-</sup>→Li<sub>x</sub>TiO<sub>2</sub>. At the same time, a new discharge peak of 1.86 V appeared in the next cycle, which was due to the lithiation process of S to Li<sub>2</sub>S:[51] S+2Li<sup>+</sup>+2e<sup>-</sup>→Li<sub>2</sub>S. Then, during charging, the two anode peaks observed near 1.63 V and 2.32 V indicated the release of Li<sup>+</sup> from Li<sub>x</sub>TiO<sub>2</sub> and the oxidation of Li<sub>2</sub>S, respectively. The CV curves remained stable after the primary charge and discharge process, indicating the excellent stability of the TiO<sub>2</sub>/NC-MoS<sub>2</sub> electrode.

The galvanostatic charge-discharge profiles of TiO<sub>2</sub>/NC-MoS<sub>2</sub> for the first three cycles are shown in Fig. 5b. During the first discharge process, the plateaus appear at 0.75 V and 0.5 V, owing to the formation of Li<sub>x</sub>MoS<sub>2</sub> and the transformation of Li<sub>x</sub>MoS<sub>2</sub> into Mo and Li<sub>2</sub>S, respectively.[52] The peak forming at 1.86 V in the subsequent discharge cycles suggests the formation of Li<sub>2</sub>S.[53] These results are also in agreement with the CV results. The CE for the electrode was calculated as 66%, with a discharge capacity of 981.2 mA h g<sup>-1</sup> and a charge capacity of 650.9 mA h g<sup>-1</sup>. The side reaction and solid electrolyte interface layer led to the loss of capacity. [54] In the 2<sup>nd</sup> cycle, the CE was 95% (668.5 vs 633.6 mA h g<sup>-1</sup>). Moreover, the overlapping charge–discharge curves indicated the superior cycling stability of the TiO<sub>2</sub>/NC-MoS<sub>2</sub> anode.

The cycling performance of the TiO<sub>2</sub>/NC-MoS<sub>2</sub> hybrid was tested at 0.1 A g<sup>-1</sup> (Fig. 5c). The specific capacity of the TiO<sub>2</sub>/NC-MoS<sub>2</sub> hybrid can be retained at 629.9 mA h g<sup>-1</sup> after 200 cycles, corresponding to 97% retention of the reversible capacity (649.4 mA h g<sup>-1</sup>). However, the TiO<sub>2</sub>/NC hybrid and MoS<sub>2</sub> exhibited relatively low discharge capacities down to 79 and 247.8 mA h g<sup>-1</sup>, respectively. Moreover, the CE of the hybrid was increased from 66% to more than 98% in the subsequent cycles. These results suggest a good cycling stability of the TiO<sub>2</sub>/NC-MoS<sub>2</sub> electrodes. TiO<sub>2</sub>/NC-MoS<sub>2</sub> could deliver values of 603.9, 566, 515.6, 465.6, 376.8 and 190.5 mA h g<sup>-1</sup> at 0.1, 0.2, 0.5, 1.0, 2.0 and 5.0 A g<sup>-1</sup>, respectively, compared to those of TiO<sub>2</sub>/NC at 70.5, 48.3, 27.2, 10.9, 2.7 and

6.7 mA h g<sup>-1</sup>. When the current density was 5 A g<sup>-1</sup>, TiO<sub>2</sub>/NC-MoS<sub>2</sub> still presented a charge specific capacity of 190.5 mA h g<sup>-1</sup>, whereas MoS<sub>2</sub> and TiO<sub>2</sub>/NC only possessed capacities of 52.1 and 6.7 mA h g<sup>-1</sup> at the same current density, respectively. The TiO<sub>2</sub>/NC-MoS<sub>2</sub> mixture maintained 471.2 mA h g<sup>-1</sup> over 1000 cycles at 1 A g<sup>-1</sup>. Compared to previous MoS<sub>2</sub>-based anode materials (Table 1), our TiO<sub>2</sub>/NC-MoS<sub>2</sub> mixture showed the best cycle stability and rate capacity. Both the activity and stability of the electrode could be improved with TiO<sub>2</sub> nanofibers, N-coated carbon, and MoS<sub>2</sub> nanosheets.[57]

**Table 1.** A comparison of the electrochemical performance of TiO<sub>2</sub> and MoS<sub>2</sub> composites as anode materials for LIBs

Electrode materials	Cycling stability after 100 cycles at current density	Rate performance	Reference
TiO <sub>2</sub> /NC-MoS <sub>2</sub> nanofibers	603.9 mA h g <sup>-1</sup> at 0.1 A g <sup>-1</sup>	603.9, 465.6, 649.4 mA h g <sup>-1</sup> at 0.1, 1.0, 0.1 A g <sup>-1</sup>	This work
TiO <sub>2</sub> /MoS <sub>2</sub> nanobelts	479.7 mA h g <sup>-1</sup> at 0.1 A g <sup>-1</sup>	495.1, 303,474 mA h g <sup>-1</sup> at 0.1, 1, 0.1 A g <sup>-1</sup>	20
TiO <sub>2</sub> @MoS <sub>2</sub> nano-onions	519 mA h g <sup>-1</sup> at 0.1 A g <sup>-1</sup>	550, 400,598 mA h g <sup>-1</sup> at 0.1, 1, 0.1 A g <sup>-1</sup>	21
TiO <sub>2</sub> /C/MoS <sub>2</sub> microspheres	621 mA h g <sup>-1</sup> at 0.1 A g <sup>-1</sup>	663, 270,664 mA h g <sup>-1</sup> at 0.1, 1, 0.1 A g <sup>-1</sup>	22
core-shell TiO <sub>2</sub> @MoS <sub>2</sub>	467 mA h g <sup>-1</sup> at 0.1 A g <sup>-1</sup>	722, 464,720 mA h g <sup>-1</sup> at 0.1, 1, 0.1 A g <sup>-1</sup>	30
MoS <sub>2</sub> /TiO <sub>2</sub> nanowire array	350 mA h g <sup>-1</sup> at 0.03 A g <sup>-1</sup>	437, 287, 399 mA h g <sup>-1</sup> at 0.03, 0.34,0.03 A g <sup>-1</sup>	54
MoS <sub>2</sub> /C/TiO <sub>2</sub> nanotube	472 mA h g <sup>-1</sup> at 0.1 A g <sup>-1</sup>	713, 461, 611 mA h g <sup>-1</sup> at 0.1, 1, 0.1 A g <sup>-1</sup>	55
MoS <sub>2</sub> /C/TiO <sub>2</sub> nanowire	544 mA h g <sup>-1</sup> at 0.1 A g <sup>-1</sup>	724, 414, 563 mA h g <sup>-1</sup> at 0.1, 1, 0.1 A g <sup>-1</sup>	56
TiO <sub>2</sub> nanowire@MoS <sub>2</sub> nanosheet	501mA h g <sup>-1</sup> at 0.1 A g <sup>-1</sup>	581, 555, 470 mA h g <sup>-1</sup> at 0.1, 0.5, 0.1 A g <sup>-1</sup>	57

The EIS test for TiO<sub>2</sub>/NC-MoS<sub>2</sub> and TiO<sub>2</sub>/NC is shown in Fig. 5f. The semicircle of the EIS curves consisted of the high-frequency region representing the charge transfer resistance and the straight sloping line at the low-frequency region showing the diffusion resistance. Compared with that of TiO<sub>2</sub>/NC and MoS<sub>2</sub>, the semicircle of TiO<sub>2</sub>/NC-MoS<sub>2</sub> was smaller, demonstrating lower interfacial and charge transfer resistance. [53] These results are attributed to the synergistic effects of the TiO<sub>2</sub> nanowires, the superior conductivity of C, and the MoS<sub>2</sub> nanosheets. First, the MoS<sub>2</sub> sheets might be convenient for lowering the activation energy for Li<sup>+</sup> diffusion and shortening the diffusion pathway. Second, N-coated carbon was beneficial to the conductivity. [58,59] Third, the TiO<sub>2</sub> nanofibers acting as a framework provided large channels for Li<sup>+</sup> insertion/extraction.

#### 4. CONCLUSION

In conclusion, MoS<sub>2</sub> nanoflakes with nitrogen-doped carbon-coated TiO<sub>2</sub> nanofibers were successfully prepared through a facile process. The TiO<sub>2</sub>/NC-MoS<sub>2</sub> nanocomposites were proved to be outstanding anode materials for LIBs due to their good cycle stability and rate capability. This favorable performance may result from the strength of TiO<sub>2</sub> and the activity of MoS<sub>2</sub> for Li<sup>+</sup> storage. The TiO<sub>2</sub>/NC-MoS<sub>2</sub> nanocomposites show promising applications in LIBs.

#### ACKNOWLEDGMENTS

We gratefully acknowledge the Natural Science Foundation of Liaoning Province (No. 2019-ZD-0266).

#### References

1. Y. Zhang, Q. Ma, S. Wang, X. Liu and L. Li, *ACS Nano*, 12(2018)4824.
2. M. Xia, Z. Zhou, Y. Su, Y. Li, Y. Wu, N. Zhou, H. Zhang and X. Xiong, *Appl. Surf. Sci.*, 467 (2019) 298.
3. X. Wang, Y. Chen, O.G. Schmidt and C. Yan, *Chem. Soc. Rev.*, 45 (2016) 1308.
4. B. Chen, Y. Meng, J. Sha, C. Zhong, W. Hu and N. Zhao, *Nanoscale*, 10 (2017)34.
5. T. Song, U. Paik, *J. Mater. Chem.*, 4 (2016)14.
6. W. An, B. Gao, S. Mei, B. Xiang, J. Fu, P. Chu and K. Huo, *Nat. Commun.*, 10(2019)1.
7. X. Wang, G. Li, M. H. Seo, F. M. Hassan and M. A. Hoque, *Adv.Energy.Mater*, 5 (2015) 1501106.
8. L. Xu, L. Ma, X. Zhou, Y. Ling, X. Wang and M. Chen, *Appl. Surf. Sci.*, 458(2018)86.
9. H. Sopha, A. Tesfaye, R. Zazpe, J. Michalicka, F. Dvorak, T. Djenizian and J. Macak, *FlatChem*, 17(2019)100130.
10. H. Li, X. Wang, B. Ding, G. Pang, P. Nie, L. Shen and X. Zhang, *ChemElectroChem*, 1(2014) 1118.
11. Y. Liu, X. He, D. Hanlon, A. Harvey, U. Khan, Y. Li and J. Coleman, *ACS Nano*, 10(2016)5980.
12. Y. Fang, Y. Lv, F. Gong, A. A. Elzatahry, G. Zheng and D. Zhao, *Adv.Mater.*, 28(2016)9385.
13. M. Cao, L. Gao, X. Lv and Y. Shen, *J. Power Sources*, 350(2017)87.
14. Y. Zhang, Y. Tang, W. Li and X. Chen, *ChemNanoMat*, 2(2016)764.
15. Q. Pang, Y. Zhao, X. Bian, Y. Ju, X. Wang, Y. Wei, B. Liu, F. Du, C. Wang and G. Chen, *J.Mater.Chem.*, 5(2017)3667.
16. L. Wu, J. Zheng, L. Wang, X. Xiong, Y. Shao, G. Wang, J.H. Wang, S. Zhong and M. Wu, *Angew. Chem. Int. Ed.*, 58(2019)811.
17. B. Chen, E. Liu, T. Cao, F. He, C. Shi, C. He, L. Ma and Q. Li, *Nanoscale*, 10(2017)34.
18. J. Li, N. Zhao, *Nano Energy*, 33(2017)247.
19. Q. Pang, Y. Zhao, X. Bian, X. Ju, X. Wang and X. Wei, *J. Mater. Chem. A.*, 5(2017)3667.
20. H. Zhou, P. Lv, X. Xia, J. Yu, Z. Pang, H. Qiao and Q. Wei, *Mater. Lett.*, 218(2018)47.
21. R. Dai, A. Zhang, Z. Pan, A. M. Al-Enizi, A. A. Elzatahry, L. Hu and G. Zheng, *Small*, 12 (2016)2792.
22. J. Zhang, Y. Li, T. Gao and X. Sun, *Ceram. Int.*, 44(2018)8550.
23. M. Zhu, Z. Luo, A. Pan, S. Liang and G. Cao, *Chem. Eng. J.*, 334(2018) 2190.
24. C. Zhu, D. Wei, Y. Wu, Z. Zhang, G. Zhang, J. Duan and Z.Chen, *J. Alloys Compd.*, 778(2019)731.
25. Y. Yuan, F. Chen, S. Yin, L. Wang, M.Zhu, J. Yang and S.Guo, *J. Power Sources*, 420(2019)38.
26. M. Wu, S. Xia and J. Ding, *ChemElectroChem*, 5(2018)2263.
27. W. Chen, J. Wang, K. Ma, M. Li, S. Guo, F. Liu and J. Cheng, *Appl. Surf. Sci.*, 451 (2018) 280.
28. X. Zhang, Q. Huang, F. Deng, H. Huang, Q. Wan, M. Liu and Y. Wei, *Appl.Mater.Today*, 7(2017), 222.

29. Y. Li, L. Liang, Y. Rui, B. Ming and Y. Wei, *ChemElectroChem*, 6(2019)1069.
30. W. Xu, T. Wang, Y. Yu, and S. Wang, *J. Alloy. Comp.*, 689(2016)460.
31. S. Ribbens, V. Meynen, G.V. Tendeloo, X. Ke, M. Mertens, B.U.W. Maes, P. Cool and E.F. Vansant, *Microporous Mesoporous Mater.*, 114(2008)401.
32. W. Song, J. Chen, X. Ji, X. Zhang, F. Xie, and D.J. Riley, *J.Mater.Chem.A.*, 4(2016)8762.
33. Z. Deng, H. Jiang, Y. Hu, Y. Liu, L. Zhang, H. Liu and C. Li, *Adv. Mater.*, 29(2017)1603020.
34. Q. Pang, Y. Zhao, X. Bian, Y. Ju, X. Wang, Y. Wei, B. Liu, F. Du, C. Wang and G. Chen, *J. Mater. Chem. A.*, 5(2017)3667.
35. W. Zhou, Z. Yin, Y. Du, X. Huang, Z. Zeng, Z. Fan, H. Liu, J. Wang and H. Zhang, *Small*, 9(2013)140.
36. C. Zhu, T. Akiyama, *Green Chem.*, 18(2016)2106.
37. B. Guo, K. Yu, H. Fu, Q. Hua, R. Qi, H. Li, H. Song, S. Guo and Z. Zhu, *J. Mater. Chem. A.*, 3(2015)6392.
38. X. Liu, Z. Xing, Y. Zhang, Z. Li, X. Wu, S. Tan, X. Yu, Q. Zhu and W. Zhou, *Appl. Catal. B: Environ.*, 11(2017)119.
39. A. Jorio, L. G. Cancado, *Phys.Chem.*, 14(2012)15246.
40. S. Sahoo, APS. Gaur, M. Ahmadi, M. Guinel and R. S. Katiyar, *J. Phys. Chem. C.*, 117(2013)9042.
41. J. Zhou, M. Guo, L. Wang, Y. Ding, Z. Zhang and S. Luo, *Chem. Eng. J.*, 366(2019)163.
42. Z. Huang, H. Hou, C. Wang, S. Li, Y. Zhang and X. Ji, *Chem. Mater.*, 29(2017)7313.
43. W. Zhuang, L. Li, J. Zhu, R. An, L. Lu, X. Lu, X. Wu and H. Ying, *ChemElectroChem*, 2(2015) 374.
44. X. Wang, H. Feng, Y. Wu and L. Jiao, *Am.Chem.Soc.*, 135(2013)5304.
45. J. Guan, X. Zhong, X. Chen, X. Zhu, P. Li, J. Wu, Y. Lu, Y. Yu and S. Yang, *Nanoscale*, 10(2018)2473.
46. H. Zhou, L. Liu, X. Wang, F. Liang, S. Bao, D. Lv, Y. Tang and D. Jia, *J. Mater.Chem.A.*, 1(2013) 8525.
47. S. Ding, D. Zhang, J. Chen and X. Lou, *Nanoscale*, 4(2012)95.
48. X.Zhou, L.Wan,Y.Guo, *ChemComm*, 49(2013)1838.
49. D. McNulty, E. Carroll and C. O'Dwyer, *Adv. Energy Mater.*, 7(2017)1602291.
50. J. Shin, J. H. Joo, D. Samuelis and J. Maier, *Chem. Mater.*, 24(2012)543.
51. K. Chang, W. Chen, *ACS Nano*, 5(2011)4720.
52. T. Stephenson, Z. Li, B. Olsen and D. Mitlin, *Energy Environ. Sci.*, 7(2014)209.
53. R. Elazari, G. Salitra, A. Garsuch, A. Panchenko and D. Aurbach, *Adv. Mater.*, 23(2011)5641.
54. J. Liao, B. De Luna and A. Manthiram, *J.Mater.Chem.A.*, 4(2016)801.
55. X Xu, Z Fan, S Ding, D Yu and Y Du, *Nanoscale*, 6(2014)5245.
56. X. Li, W. Li, M. Li, P. Cui, D. Chen, T. Gengenbach, L. Chu, H. Liu and G. Song, *J. Mater. Chem. A.*, 3(2015)2762.
57. S. Wang, B. Guan, L. Yu and X. Lou, *Adv. Mater.*, 29(2017)1702724.
58. K. He, F. Lin, Y. Zhu, X. Yu, J. Li, R. Lin, D. Nordlund, T. Weng, R. M. Richards, X. Yang, M. M. Doeff, E. A. Stach, Y. Mo, H. Xin and D. Su, *Nano Lett.*, 15(2015)5755.
59. D. Wang, L. Liu, S. Zhao, Z. Hu and H. Liu, *J.Phys.Chem.C.*, 120(2016)4779.